Research Square

Preprints are preliminary reports that have not undergone peer review.
They should not be considered conclusive, used to inform clinical practice,
or referenced by the media as validated information.

High-pressure behaviour of REE-free calcioburbankite structure

Sergey V. Rashchenko

rashchenko@igm.nsc.ru

Sobolev Institute of Geology and Mineralogy SB RAS

Anna Yu. Likhacheva

Sobolev Institute of Geology and Mineralogy SB RAS

Alexandr V. Romanenko

Sobolev Institute of Geology and Mineralogy SB RAS

Anton F. Shatskiy

Vernadsky Institute of Geochemistry and Analytical Chemistry of the Russian Academy of Science

Research Article

Keywords: calcioburbankite, carbonate, high pressure

Posted Date: August 13th, 2026

DOI: https://doi.org/10.21203/rs.3.rs-10589323/v1

License: This work is licensed under a Creative Commons Attribution 4.0 International License. Read Full License

Additional Declarations: No competing interests reported.

Abstract

The high-pressure behaviour of REE-free calcioburbankite, $Na_2Ca_4(CO_3)_5$, was investigated by *in situ* single-crystal X-ray diffraction at ambient temperature to ~ 20 GPa. The phase remains stable throughout the experimental range and exhibits pronounced compressional anisotropy, with the *c* axis (linear modulus M_0 = 158(3) GPa) substantially more compressible than the *a* axis (linear modulus M_0 = 239.8(18) GPa). The pressure-volume data are well fitted by a 3rd order Birch-Murnaghan equation of state with V_0 = 584.12(16) Å^3, K_0 = 68.1(7) GPa and K'_0 = 5.26(13). Structural analysis shows that compression is accommodated chiefly by contraction of the cation kagome-layer stacking and can be described both from the point of view of 'perovskite' tesselation tiles and from the conventional point of view of cation-centred coordination polyhedra. The results define the elastic response of the REE-free end-member of calcioburbankite and provide constraints relevant to modelling burbankite-group minerals under mantle conditions.

Introduction

Double Na-Ca and K-Ca carbonates with a common formula $A_nCa_m(CO_3)_{m+n/2}$ (*A* = Na, K) now attract a lot of attention as potential subsolidus phases which control melting temperatures and composition of melt for carbonated rocks subducted down to the mantle transition zone (MTZ). The latter follows not only from experimental works, which have demonstrated the appearance of such phases in subsolidus assemblages of carbonated pelites (Grassi and Schmidt 2011), eclogites (Kiseeva et al. 2013; Thomson et al. 2016) and peridotites (Litasov et al. 2013) at MTZ pressures, but also from mineralogy of inclusions in kimberlitic minerals (Giuliani et al. 2012; Golovin et al. 2016; Logvinova et al. 2019) and even 'super-deep' diamonds (Kaminsky et al. 2016), which often contains double Na-Ca and K-Ca carbonates.

Among numerous high-pressure Na-Ca and K-Ca carbonates synthesised experimentally (Gavryushkin et al. 2014; Rashchenko et al. 2017, 2018, 2024; Ignatov et al. 2024; Likhacheva et al. 2025), hexagonal ($P6_3mc$) $Na_2Ca_4(CO_3)_5$ phase (Rashchenko et al. 2017) is the only one with a known mineral analogue, namely, calcioburbankite $(Na,Ca,REE)_3(Ca,REE,Sr)_3(CO_3)_5$ (Van Velthuizen et al. 1995; Belovitskaya et al. 2001). The formula of the phase can be also written in the structural notation $M1_3M2_3(CO_3)_5$ as $(Na_2Ca)Ca_3(CO_3)_5$ indicating that M1 cation site is occupied by Na and Ca, whereas M2 site – purely by Ca. Since the occurrence of REE in the calcioburbankite structure is controlled by the $2Ca^{2+} \leftrightarrow Na^+ + REE^{3+}$ heterovalent substitution, the $Na_2Ca_4(CO_3)_5$ phase can be considered as a REE-free end-member of the corresponding solid solution. Studies of the Na_2CO_3-$CaCO_3$ binary demonstrate that such a composition becomes thermodynamically stable at pressures of ~ 6 GPa (Shatskiy et al. 2013; Podborodnikov et al. 2018), whereas origin of natural calcioburbankites is characterized by much lower pressures (Belovitskaya and Pekov 2004). The latter demonstrate that admixture of REE and large alkali-earth cations (Sr, Ba), typical for natural samples, stabilises the structure, otherwise stable at high-pressures only. The possibility of burbankite group minerals to accommodate REE cations suggests its important role in the formation of REE deposits, as soon as the corresponding mineral assemblages often compositionally represent the products of dissolution of burbankite group minerals by hydrothermal fluids (Broom-Fendley 2024).

The reported structural study of high-pressure behaviour of REE-free calcioburbankite hence provide constraints on the stability and thermodynamic properties of $Na_2Ca_4(CO_3)_5$ end member under mantle pressures and may be also useful for the development of thermodynamic models for solid solutions between burbankite group minerals. It supplements the recent high-pressure Raman study of $Na_2Ca_4(CO_3)_5$ up to ~ 24 GPa, where its stability up to MTZ pressures (at least at ambient temperature) was reported (Rashchenko et al. 2023).

Experimental

The $Na_2Ca_4(CO_3)_5$ sample was synthesized from a stoichiometric mixture of pure Na_2CO_3 and CaCO3 (Wako) in a Kawai-type multianvil apparatus at Tohoku University (Sendai, Japan). The high-pressure cell assemblage and experimental details are described in (Shatskiy et al. 2013). The mixture was ground in an agate mortar under acetone and loaded into a graphite capsule, which then was dried at 300°C for 3 h and stored in a drying oven prior to experiment. During the synthesis, the sample was compressed to a pressure of 6 GPa at room temperature, heated to 1050°C for 19 h, and then quenched by cutting off the electrical power of the heater, followed by slow decompression. Chemical composition, Raman spectra and crystal structure of $Na_2Ca_4(CO_3)_5$ at ambient pressure were reported in (Rashchenko et al. 2017).

The *in situ* high pressure single-crystal diffraction experiments were performed at the station ID015B at the European Synchrotron Radiation Facility. Membrane driven LeToullec type diamond anvil cell (DAC) was used, equipped with Boehler-Almax anvils with an opening half-angle of 32°. The culet diameter was 600 μm. Stainless steel was used as the gasket material, indented to about 80 μm and drilled to obtain a sample chamber with diameter of 350 μm. A small (~ 60×40×20 μm) platelet crushed from a single-crystal fragment of the $Na_2Ca_4(CO_3)_5$ sample was placed inside the sample chamber along with ruby sphere for pressure measurement and tungsten chip for beam centring (Fig. 1).

Hydrostatic conditions were provided by the DAC loading with a helium pressure-transmitting medium. A measurement at ambient pressure was made first, and then the DAC was loaded with He and sequentially pressurized up to ~ 20 GPa; after decompression one more measurement at ambient pressure was performed. Pressures were determined using ruby fluorescence scale (Shen et al. 2020) before (P_{start}) and after (P_{end}) each diffraction measurement (Table 1); a standard uncertainty σ of average pressure (P_{ave}) was estimated from $\sigma^2 = S^2 + 0.05^2$, where S^2 is an unbiased sample variance of P_{start} and P_{end}, whereas 0.05 GPa corresponds to a typical precision of spectrometer. Monochromatic X-ray diffraction measurements were performed at a wavelength of 0.41505 Å with a beam size of ~ 10×10 μm (Merlini and Hanfland 2013). Diffraction patterns were collected using a MAR555 flat panel detector during ± 32° rotation of the DAC in 0.5° steps with 1 s exposure. The patterns were then transferred into CrysAlisPro software using ESPERANTO protocol (Rothkirch et al. 2013) for indexing and integration. A crystallographic computing system JANA2020 (Petříček et al. 2023) was used for structure refinement on the basis of ambient pressure model from (Rashchenko et al. 2017); no phase transitions were observed in the studied pressure range in accordance with the recent high-pressure Raman study (Rashchenko et al. 2023). The crystal structures were refined on F^2 at 22 pressure points with anisotropic displacement parameters. A brief experimental summary is given in Table 1, all remaining information regarding data collection and refinement is embedded into a supplementary CIF.

Table 1
Experimental summary. The 'data' column corresponds to datablock names in the CIF; R_{int}, R_1, wR_2 and GooF – to CIF entries _diffrn_reflns_av_r_equivalents, _refine_ls_r_factor_all, _refine_ls_wr_factor_ref and _refine_ls_goodness_of_fit_ref, respectively.

data	P_{start}, GPa	P_{end}, GPa	P_{ave}, GPa	*a*, Å	*c*, Å	*V*, Å^3	R_{int}	R_1	wR_2	GooF
p0	10^{-4}	10^{-4}	10^{-4}	10.378(2)	6.260(2)	583.8(2)	0.036	0.036	0.091	1.6
p1	1.06	1.06	1.06(5)	10.334(2)	6.218(2)	575.1(2)	0.053	0.038	0.084	1.3
p2	2.01	2.07	2.04(6)	10.296(2)	6.188(2)	568.1(2)	0.048	0.041	0.095	1.3
p3	3.03	3.04	3.04(5)	10.258(2)	6.146(2)	560.1(2)	0.037	0.029	0.067	1.2
p4	4.00	4.21	4.11(12)	10.225(2)	6.123(2)	554.4(2)	0.041	0.036	0.085	1.3
p5	5.08	5.11	5.10(5)	10.194(2)	6.092(2)	548.2(2)	0.040	0.034	0.075	1.3
p6	6.05	6.06	6.06(5)	10.166(2)	6.066(2)	542.9(2)	0.029	0.029	0.067	1.4
p7	6.97	6.99	6.98(5)	10.137(2)	6.044(2)	537.9(2)	0.040	0.034	0.082	1.4
p8	8.03	8.08	8.06(6)	10.110(2)	6.013(2)	532.3(2)	0.033	0.025	0.060	1.2
p9	8.96	9.01	8.99(6)	10.086(2)	5.995(2)	528.1(2)	0.037	0.031	0.072	1.2
p10	9.96	10.01	9.99(6)	10.061(2)	5.975(2)	523.8(2)	0.043	0.032	0.081	1.4
p11	11.01	11.07	11.04(6)	10.037(2)	5.946(2)	518.7(2)	0.029	0.029	0.070	1.5
p12	11.98	12.02	12.00(5)	10.016(2)	5.928(2)	515.0(2)	0.031	0.025	0.057	1.2
p13	13.04	13.05	13.05(5)	9.992(2)	5.908(2)	510.8(2)	0.042	0.033	0.081	1.4
p14	14.02	14.01	14.02(5)	9.969(2)	5.886(2)	506.6(2)	0.040	0.034	0.078	1.3
p15	14.95	14.94	14.95(5)	9.952(2)	5.874(2)	503.9(2)	0.028	0.026	0.059	1.3
p16	16.00	16.03	16.02(5)	9.931(2)	5.854(2)	500.0(2)	0.028	0.026	0.057	1.2
p17	17.06	17.06	17.06(5)	9.910(2)	5.830(2)	495.9(2)	0.029	0.025	0.061	1.3
p18	18.11	18.16	18.14(6)	9.889(2)	5.816(2)	492.6(2)	0.029	0.027	0.063	1.4
p19	19.10	19.16	19.13(6)	9.873(2)	5.799(2)	489.6(2)	0.029	0.046	0.192	4.1
p20	19.97	19.97	19.97(5)	9.860(2)	5.786(2)	487.1(2)	0.028	0.024	0.056	1.3
p21	10^{-4}	10^{-4}	10^{-4}	10.379(2)	6.266(2)	584.6(2)	0.035	0.031	0.070	1.2

Dependencies of unit cell volume and linear dimensions on pressure were quantified using Birch-Murnaghan equation of state (EOS) (Birch 1947); the fitting of EOS parameters to the obtained *PV*-data was performed using Scipy implementation of a weighted orthogonal distance regression algorithm (Zwolak et al. 2007) embedded into the 'eos.py' module of 'crystchemlib' Python library (Rashchenko 2025). The obtained parameters were verified using a *de facto* standard tool of high-pressure crystallographic community 'EosFit'

(Gonzalez-Platas et al. 2016). Volumes of 'perovskite' tiles were calculated using crystchemlib tools (see a supplementary Jupyter notebook), for volumes of cation-centred coordination polyhedra 'Crystal Palace' software was implemented (Angel et al. 2025).

Results and discussion

Crystal structure of calcioburbankite

Because of high coordination number and low symmetry of the M1 and M2 cation sites in the calcioburbankite structure (or, generally speaking, burbankite structure type), its traditional representation using cation-centred coordination polyhedra does not result in a clear description and visualization of the structure. Here an alternative way is proposed based on geometry of cation sites packing, inspired by ideas of O'Keeffe and Hyde (O'Keeffe and Hyde 1985).

The arrangement of M1 and M2 cation sites in (001) planes of calcioburbankite structure corresponds to plane 'kagome' nets, alternating along the [001] direction (Fig. 2). Two such nets, built of M1 atoms are situated at $z \approx 0.02$ and $z \approx 0.52$, while a pair of nets built of M2 atoms – at $z \approx 0.33$ and $z \approx 0.83$. Each pair is connected by 6_3 screw axis, passing through the unit cell origin (shown in Fig. 2). However, for kagome net of M1 atoms the 6_3 screw axis passes through hexagonal 'loop' so that symmetrically equivalent nets have the same orientation, whereas for M2 kagome net the screw axis passes through triangular loop and symmetrically equivalent nets have an opposite orientation.

One can notice that each hexagonal loop of cation kagome net is always 'sandwiched' between two triangular loops of neighbour nets. Such a stacking rule generally holds for perovskite (*sensu lato*) polytypes and the sequence of kagome nets in the calcioburbankite structure correspond to that in the 4H-polytype of perovskite with $P6_3/mmc$ symmetry (Kunz et al. 2024). The latter also explains a pronounced $P6_3/mmc$ pseudosymmetry of cation sites in $Na_2Ca_4(CO_3)_5$: the absolute displacements of M1 and M2 sites from a $P6_3/mmc$ supergroup structure are 0.4 and 0.3 Å, respectively, as calculated by PSEUDO (Capillas et al. 2011). However, an 'ideal' c/a ratio of 4H-perovskites $\sqrt{8/3} \approx 1.63$ significantly exceeds that of $Na_2Ca_4(CO_3)_5$ ($c/a \approx 0.60$). In Fig. 3 the crystal structure of $Na_2Ca_4(CO_3)_5$ is 'stretched' along the c direction up to the c/a ratio of $\sqrt{8/3}$ for better visual comparison with α-$SrMnO_3$ 4H-perovskite (Kuroda et al. 1981).

A perovskite-type stacking of kagome nets tessellates crystal structure space into three types of tiles:

- octahedral tile (blue in Fig. 3) is formed by oppositely oriented triangular loops of neighbour nets;
- cubic cuboctahedral tile (red in Fig. 3) is formed by a hexagonal loop of kagome net sandwiched between oppositely oriented triangular loops of neighbour nets;
- hexagonal cuboctahedral tile (green in Fig. 3) is formed by a hexagonal loop of kagome net sandwiched between equally oriented triangular loops of neighbour nets.

A total number of cuboctahedral tiles always equals that of octahedral tiles, resulting in a well-known ABX_3 formula of perovskites, where A denotes species occupying cuboctahedral tiles, B – species occupying octahedral tiles and X – species of kagome nets.

Strictly speaking, the $Na_2Ca_4(CO_3)_5$ structure should be classified as 4H-antiperovskite as soon as its kagome nets are built of cations instead of anions. Accordingly, the described above tiles are occupied by $(CO_3)^{2-}$ anions in the following way (see also Fig. 4):

- the cubic cuboctahedron (hereafter *A*1 tile, red in Figs. 3–4) is populated by carbonate anion of C1 atom;
- the hexagonal cuboctahedron (hereafter *A*2 tile, green in Figs. 3–4) is populated by a cluster of three carbonate anions of C2 atoms;
- half of octahedral tiles (hereafter *B*1, blue in Figs. 3–4) are populated by carbonate anions of C3 atom;
- half of octahedral tiles (hereafter *B2*, empty in Figs. 3–4) are unoccupied.

Note that Fig. 4 is plotted without artificial 'stretching' along the *c* direction and demonstrates actual geometry of the tiles, strongly flattened in the *c* direction compared with ideal cuboctahedra and octahedra. Such a deformation, however, agrees with a planar geometry of $(CO_3)^{2-}$ species, populating the tiles, whereas in 'normal' perovskites the tiles are typically occupied by spherical ions or more or less isometric organic molecules.

The proposed description of burbankite structure type is particularly useful for establishing structural relationships with other compounds which demonstrate the same cation arrangement combined with diversity of species, populating the tiles. *E.g.*, in $Cs_3Ba_4(CO_3)_3F_5$ compound (Zou et al. 2011) *A*1 tiles are populated by single F^- anions, *A*2 tiles – by $[Ba(CO_3)_3]^{4-}$ clusters and *B*2 tiles – by $[F_4]^{4-}$ clusters. Borate compounds of burbankite structure type are even more flexible, in addition to $(BO_3)^{3-}$ anions incorporating F^-, Cl^-, Br^- and CN^- in *A*1 tiles, $[Ba(BO_3)_3]^{7-}$ and $[Sr(BO_3)_3]^{7-}$ clusters in *A*2 tiles, $[F_4]^{4-}$, $[(BO_3)F]^{4-}$ and even $[SiO_4]^{4-}$ in *B*2 tiles (Rashchenko and Bekker 2021). Such a flexibility of the structure type, currently acknowledged predominantly in materials science, highlights the role of burbankite group minerals in concentration and transport of volatiles and rare elements.

PV-equation of state

Among the variety of burbankite group minerals, currently only $Na_3Ca_2La(CO_3)_5$ calcioburbankite has been structurally studied at high pressures; in the corresponding work of S. Milani and coauthors (Milani et al. 2022) behaviour of unit cell parameters and crystal structure at pressures up to ~ 7 GPa are discussed. In particular, the *PV*-data for $Na_3Ca_2La(CO_3)_5$ were fitted by the 2nd order Birch-Murnaghan equation of state (EoS) with zero-pressure unit cell volume V_0 = 593.22(3) $Å^3$ and bulk modulus K_0 = 69.8(4) GPa.

An increased pressure range (up to ~ 20 GPa) and less pronounced scatter in our experimental data for REE-free $Na_2Ca_4(CO_3)_5$ calcioburbankite allowed considering higher orders of the Birch-Murnaghan EoS (Table 2). A drastic decrease in the residual variance (*RV*, also referred as 'weighted chi-squared' in 'EosFit' software), corresponding to the expansion form the 2nd to the 3rd order, indicates that the K'_0 derivative does significantly deviate from the implied value of 4.

Table 2
Parameters of Birch-Murnaghan EoS for REE-free calcioburbankite $Na_2Ca_4(CO_3)_5$

Order	V_0, Å^3	K_0, GPa	K'_0	K''_0, GPa^{-1}	ΔP_{max}	Residual variance, *RV*	Degrees of freedom, μ
2	583.4(4)	75.6(6)	4*		0.40(5)	9.903	22 − 2 = 20
3	584.12(16)	68.1(7)	5.26(13)	−0.10*	−0.15(5)	1.333	22 − 3 = 19
4	584.18(16)	65.8(16)	6.4(8)	−0.36(19)	−0.12(5)	1.228	22 − 4 = 18
*Implied (not refined)							

As soon as further expansion to the 4th order results only in a moderate decrease in the residual variance, a statistic test should be applied in order to decide whether a more complex model *B* (here the 4th order expansion of the Birch-Murnaghan EoS) should be preferred over a less complex one *A* (here the ^{3rd} order expansion). We used the simplest F-test, based on the following statistics:

$$F = \frac{RV_A \cdot \mu_A - RV_B \cdot \mu_B}{RV_B \cdot (\mu_A - \mu_B)}$$

where *RV* and μ denote residual variance and degrees of freedom (*i.e.* number of experimental points minus number of refined parameters) for each model. The resulting *F* (in our case ≈ 2.6) then should be compared with a tabulated critical value of Fisher-Snedecor distribution with $\mu_A - \mu_B$ and μ_B degrees of freedom. In our case the critical value for 0.05 significance level is ≈ 4.4, which suggests that the decrease in the residual variance observed for the expansion from the 3rd to the 4th order is insignificant and the less complex 3rd order model should be preferred. The *PV*-data and equations of state for $Na_3Ca_2La(CO_3)_5$ (Milani et al. 2022) and REE-free $Na_2Ca_4(CO_3)_5$ (this work) calcioburbankites are shown in Fig. 5a; Figs. 5b-c compare different orders of $Na_2Ca_4(CO_3)_5$ EoS using deviation of observed pressures from EoS-predicted (Fig. 5b) and dependence of normalized pressure on finite Eulerian strain (Fig. 5c).

Although the unit cell volume of the La-enriched sample exceeds that of our REE-free sample by ~ 1.6%, their *PV*-points go almost parallel in the range up to 7 GPa (Fig. 5a). Higher compressibility of the $Na_3Ca_2La(CO_3)_5$ above 7 GPa predicted by the 2ndnd order Birch-Murnaghan EoS of (Milani et al. 2022) therefore seems to be an extrapolation artefact raising from the underestimated K'_0 parameter, fixed to 4 by the truncation of EoS to the 2nd order. We suggest that actual K'_0 of the $Na_3Ca_2La(CO_3)_5$ calcioburbankite should be closer to the value of 5.26(13), obtained for our REE-free $Na_2Ca_4(CO_3)_5$ sample, so that equations of state for both phases would actually differ only in the V_0 parameter.

Compressional anisotropy of REE-free $Na_2Ca_4(CO_3)_5$ calcioburbankite was estimated by fitting a^3 and c^3 with the Birch-Murnaghan EoS. For a^3 the 3rd order Birch-Murnaghan EoS was find to be statistically justified with following linear equivalents of its parameters: a_0 = 10.3781(7) Å, M_0 = 239.8(18) GPa, M'_0 = 19.1(4). For c^3 the 2rd order Birch-Murnaghan EoS was find to be statistically justified with following linear equivalents of its parameters: c_0 = 6.2616(16) Å, M_0 = 158(3) GPa, M'_0 = 12 (implied). Hence, the $Na_2Ca_4(CO_3)_5$ structure is ~ 1.5

times more compressible along the *c* axis, which agrees with its 'layered' cation arrangement highlighted in the previous section.

Compressibility of 'perovskite' tiles

As soon as burbankite-type structures can be described in terms of flattened cuboctahedral (*A*1 and *A*2) and octahedral (*B*1 and *B*2) tiles, the compressibility of $Na_2Ca_4(CO_3)_5$ structure can be 'decomposed' into compressibility of these tiles, shown in Fig. 6a-b and Table 3.

While *A*1, *A*2 and *B*2 tiles demonstrate similar compressibility, which can be described by the 3rd[rd] order of Birch-Murnaghan EoS with K_0 of 70–80 GPa, *B*1 tile populated by carbonate anion of C3 atom is much 'softer' with K_0 of 35 GPa only. Moreover, the compression of *B*1 tile is statistically better described by the 4[th] order of Birch-Murnaghan EoS (see the supplementary Jupyter notebook for the details of the analysis). The latter can be attributed to pressure-induced variation in relative distance between neighbor kagome nets of M1 and M2 cations (Fig. 2): while at ambient pressure the kagome nets forming *B*1 tiles are separated by ~ 0.19·*c*, at ~ 20 GPa these nets approach to the distance of ~ 0.176·*c* (Fig. 6c).

Table 3
Parameters of Birch-Murnaghan equations of state for 'perovskite' tiles in $Na_2Ca_4(CO_3)_5$ structure

A1	V_0, Å^3	K_0, GPa	K'_0	K''_0, GPa^{-1}
	116.27(6)	**73.6(11)**	**5.14(16)**	**−0.09***
A2	124.74(5)	69.7(9)	5.31(14)	−0.10*
B1	22.64(3)	35(3)	8.0(12)	−1.3(7)
B2	28.38(3)	79.5(19)	5.1(3)	−0.08*
*Implied (not refined)				

Although the discussed 'perovskite' tiles may seem somewhat artificial and far from conventional cation-centred polyhedra, they have an important geometrical property, being a tessellation of the crystal structure space. The latter results in additivity of their individual compressibilities $\beta_i = K_i^{-1}$, which sum exactly into the overall volume compressibility $\beta = K^{-1}$ of the crystal structure:

$$K^{-1} = \sum K_i^{-1} \cdot \frac{V_i}{V}$$

where V_i is volume of i^{th} type of tiles per unit cell and V is the unit cell volume.

- *'Anomalous' compressibility of cation-centred polyhedra*

To analyse a response of ionic bonding on pressure, one nevertheless needs to consider the conventional cation-centred polyhedra. In the case of $Na_3Ca_2La(CO_3)_5$ calcioburbankite it was found that bulk modulus of smaller $M1O_8$ coordination polyhedron (K_0 ≈ 54 GPa) does not exceed that of larger $M2O_{10}$ one (K_0 ≈ 72 GPa)

as it can be expected (Milani et al. 2022). Behaviour of $M1O_8$ and $M2O_{10}$ polyhedra in $Na_2Ca_4(CO_3)_5$ structure (Fig. 7) confirms the latter observation with K_0 being 53.3 and 69.7 GPa, respectively (Table 4).

Table 4
Parameters of $M1O_8$ and $M2O_{10}$ coordination polyhedra in calcioburbankites (for $Na_3Ca_2La(CO_3)_5$ an idealised population of cation sites is shown)

			z_c	V_0, Å^3	K_0, GPa	K'_0	d, Å	K_{HF}, GPa
M1	This work	$Na_{2/3}Ca_{1/3}$	4/3	25.550(18)	53.3(11)	5.34(19)	2.452	68
	Milani *et al.*, 2022	Na	1	26.03(4)	53.9(12)*	4**	2.458	51
M2	This work	Ca	2	37.43(3)	69.7(11)	4.96(17)	2.609	84
	Milani *et al.*, 2022	$Ca_{2/3}La_{1/3}$	7/3	38.07(3)	76.4(10)*	4**	2.622	97

*Recalculated with a minor difference from the values reported in the original publication (K_0 = 54(2) and 72(3) GPa for M1 and M2, respectively)

**Implied (not refined)

However, the empirical rule of Hazen and Finger cited in (Milani et al. 2022) is not limited by the statement that 'bulk modulus of coordination polyhedron is inversely proportional to its volume'. Strictly speaking, the corresponding formula for bulk modulus K_{HF} of cation-oxygen polyhedra (in GPa) can be written as

$$K_{HF} \approx 750 \cdot \frac{z_c}{d^3}$$

where z_c is a charge of the cation and d is an average bond length (in Å) in the polyhedron (Hazen and Finger 1979). Being applied to $Na_3Ca_2La(CO_3)_5$ and $Na_2Ca_4(CO_3)_5$ calcioburbankites (Table 4) this formula demonstrates that the observed higher bulk modulus of $M2O_{10}$ polyhedron is not an 'anomaly' but a direct consequence of higher M2 cation charge. Interestingly, the bulk modulus of $M2O_{10}$ polyhedron predicted by the Hazen-Finger rule for $Na_3Ca_2La(CO_3)_5$ with z_c = 7/3 (~ 97 GPa) even exceeds that observed experimentally (~ 76 GPa). The latter suggests that the idealized 7/3 value for z_c may be overestimated, *i.e.* a certain amount of Na^+ actually populate the M2 site or cation stoichiometry deviates from the ideal Na_3Ca_2La. The ratio of polyhedral bulk moduli hence can be used as an additional restraint in the refinement of cation sites occupancy.

Conclusions

REE-free calcioburbankite, $Na_2Ca_4(CO_3)_5$, is structurally stable to at least 20 GPa at ambient temperature, demonstrating that the burbankite-type structures can persist under mantle-relevant pressures. Compression is anisotropic and reflects the layered cation arrangement of the structure, with the *c*-axis response greater than that of the *a* axis. The structural compressibility is not uniform both from the point of view of 'perovskite' tesselation tiles (the *B*1 tile is distinctly softer than the other ones) and from the conventional point of view of

cation-centred coordination polyhedra (a larger $M2O_{10}$ polyhedron is stiffer than a smaller $M1O_8$). The latter is consistent with the higher charge of the M2 cation site and does not require invoking ‘anomalous’ bonding effects. The reported data provide a reference equation of state for the REE-free calcioburbankite end-member and a useful basis for interpreting the pressure behaviour of burbankite-group solid solutions.

Declarations

Ethics declaration

Not applicable

Funding

This study is financially supported by the grant of the Russian Scientific Foundation # 25-27-00597.

Author Contribution

A.S. synthesized the sample; S.R., A.L. and A.R. carried out the in situ high-pressure experiment; S.R. wrote the main manuscript text and prepared figures. All authors reviewed the manuscript.

Acknowledgement

This study is financially supported by the grant of the Russian Scientific Foundation # 25-27-00597. Diffraction experiments were carried at the European Synchrotron Radiation Facility and supported by approval of ESRF Proposal ES-810; Dr. Ines Collings is acknowledged for her kind assistance during the beamtime.

Data Availability

The reduced XRD data (as hkl intensities) and structural parameters of all refined crystal structures are embedded in the Supplementary CIF; the raw data are available on an appropriate request.

References

1. Angel RJ, Mazzucchelli ML, Baratelli L et al (2025) Uncertainties of recalculated bond lengths, angles and polyhedral volumes as implemented in the Crystal Palace program for parametric crystal structure analysis. Acta Crystallogr Sect Found Adv 81:202–210. https://doi.org/10.1107/S2053273325002682
2. Belovitskaya YV, Pekov IV, Gobechiya ER et al (2001) Crystal structure of calcioburbankite and the characteristic features of the burbankite structure type. Crystallogr Rep 46:927–931. https://doi.org/10.1134/1.1420820
3. Belovitskaya YV, Pekov IV (2004) Genetic mineralogy of the burbankite group. New Data Min 39:50–64

4. Birch F (1947) Finite Elastic Strain of Cubic Crystals. Phys Rev 71:809–824. https://doi.org/10.1103/PhysRev.71.809
5. Broom-Fendley S (2024) Out of sight burbankite. Nat Geosci 17:284–284. https://doi.org/10.1038/s41561-024-01410-8
6. Capillas C, Tasci ES, De La Flor G et al (2011) A new computer tool at the Bilbao Crystallographic Server to detect and characterize pseudosymmetry. Z Für Krist 226:186–196. https://doi.org/10.1524/zkri.2011.1321
7. Gavryushkin PN, Bakakin VV, Bolotina NB et al (2014) Synthesis and Crystal Structure of New Carbonate $Ca_3Na_2(CO_3)_4$ Homeotypic with Orthoborates $M_3Ln_2(BO_3)_4$ (M = Ca, Sr, and Ba). Cryst Growth Des 14:4610–4616. https://doi.org/10.1021/cg500718y
8. Giuliani A, Kamenetsky VS, Phillips D et al (2012) Nature of alkali-carbonate fluids in the sub-continental lithospheric mantle. Geology 40:967–970
9. Golovin AV, Sharygin IS, Korsakov AV (2016) Origin of alkaline carbonates in kimberlites of the Siberian craton: Evidence from melt inclusions in mantle olivine of the Udachnaya-East pipe. Chem Geol. https://doi.org/10.1016/j.chemgeo.2016.10.036
10. Gonzalez-Platas J, Alvaro M, Nestola F, Angel R (2016) EosFit7-GUI: a new graphical user interface for equation of state calculations, analyses and teaching. J Appl Crystallogr 49:1377–1382. https://doi.org/10.1107/S1600576716008050
11. Grassi D, Schmidt MW (2011) The Melting of Carbonated Pelites from 70 to 700 km Depth. J Petrol 52:765–789. https://doi.org/10.1093/petrology/egr002
12. Hazen RM, Finger LW (1979) Bulk modulus—volume relationship for cation-anion polyhedra. J Geophys Res Solid Earth 84:6723–6728. https://doi.org/10.1029/JB084iB12p06723
13. Ignatov MA, Rashchenko SV, Likhacheva AY et al (2024) High-pressure structural behavior of α-K2Ca3(CO3)4 up to 20 GPa. Phys Chem Min 51:30. https://doi.org/10.1007/s00269-024-01292-7
14. Kaminsky FV, Ryabchikov ID, Wirth R (2016) A primary natrocarbonatitic association in the Deep Earth. Mineral Petrol 110:387–398. https://doi.org/10.1007/s00710-015-0368-4
15. Kiseeva ES, Litasov KD, Yaxley GM et al (2013) Melting and Phase Relations of Carbonated Eclogite at 9–21 GPa and the Petrogenesis of Alkali-Rich Melts in the Deep Mantle. J Petrol 54:1555–1583. https://doi.org/10.1093/petrology/egt023
16. Kunz SL, Haefner M, Clemens O (2024) Hexagonal Perovskites: From Stacking Sequence to Space Group Symmetry and New Opportunities. Chem Mater 36:11341–11358. https://doi.org/10.1021/acs.chemmater.4c01789
17. Kuroda K, Ishizawa N, Mizutani N, Kato M (1981) The crystal structure of α-SrMnO3. J Solid State Chem. https://doi.org/10.1016/0022-4596(81)90059-1
18. Likhacheva AY, Rashchenko SV, Ignatov MA et al (2025) Novel dense crystal structure of high-pressure synthetic K8Ca3(CO3)7 as described through cation–carbon nets. Acta Crystallogr Sect B Struct Sci Cryst Eng Mater 81. https://doi.org/10.1107/S2052520625007929
19. Litasov KD, Shatskiy A, Ohtani E, Yaxley GM (2013) Solidus of alkaline carbonatite in the deep mantle. Geology 41:79–82. https://doi.org/10.1130/G33488.1

20. Logvinova AM, Shatskiy A, Wirth R et al (2019) Carbonatite melt in type Ia gem diamond. Lithos 342–343:463–467. https://doi.org/10.1016/j.lithos.2019.06.010
21. Merlini M, Hanfland M (2013) Single-crystal diffraction at megabar conditions by synchrotron radiation. High Press Res 33:511–522. https://doi.org/Doi%2010.1080/08957959.2013.831088
22. Milani S, Spartà D, Fumagalli P, et al (2022) High-pressure and high-temperature structure and equation of state of $Na_3Ca_2La(CO_{3)5}$ burbankite. Eur J Mineral 34:351–358. https://doi.org/10.5194/ejm-34-351-2022
23. O'Keeffe M, Hyde BG (1985) An alternative approach to non-molecular crystal structures with emphasis on the arrangements of cations. Cation Ordering and Electron Transfer. Springer, Berlin Heidelberg, Berlin, Heidelberg, pp 77–144
24. Petříček V, Palatinus L, Plášil J, Dušek M (2023) Jana2020 – a new version of the crystallographic computing system Jana. Z Für Krist - Cryst Mater 238:271–282. https://doi.org/10.1515/zkri-2023-0005
25. Podborodnikov IV, Shatskiy A, Arefiev AV et al (2018) The system Na2CO3–CaCO3 at 3 GPa. Phys Chem Min 45:773–787. https://doi.org/10.1007/s00269-018-0961-2
26. Rashchenko S, Mikhno A, Shatskiy A (2023) High-pressure Raman study of Na-Ca burbankite—A possible CO_2 host in deep mantle. J Raman Spectrosc 54:101–106. https://doi.org/10.1002/jrs.6463
27. Rashchenko SV (2025) crystchemlib: a Python library and GUI for analysis of crystal structure datasets. J Appl Crystallogr 58:290–295. https://doi.org/10.1107/S1600576724011956
28. Rashchenko SV, Bakakin VV, Shatskiy AF et al (2017) Noncentrosymmetric Na2Ca4(CO3)5 Carbonate of m13M23XY3Z Structural Type and Affinity between Borate and Carbonate Structures for Design of New Optical Materials. Cryst Growth Des 17:6079–6084. https://doi.org/10.1021/acs.cgd.7b01161
29. Rashchenko SV, Bekker TB (2021) CRYSTAL CHEMISTRY OF NOVEL ANTIZEOLITE STRUCTURES. J Struct Chem 62:1935–1945. https://doi.org/10.1134/S002247662112012X
30. Rashchenko SV, Ignatov MA, Shatskiy AF et al (2024) Coupling between cation and anion disorder in β-$K_2Ca_3(CO_3)_4$. J Appl Crystallogr 57:665–669. https://doi.org/10.1107/S1600576724002292
31. Rashchenko SV, Shatskiy AF, Arefiev AV et al (2018) $Na_4Ca(CO_3)_3$: a novel carbonate analog of borate optical materials. CrystEngComm 20:5228–5232. https://doi.org/10.1039/C8CE00745D
32. Rothkirch A, Gatta GD, Meyer M et al (2013) Single-crystal diffraction at the Extreme Conditions beamline P02.2: procedure for collecting and analyzing high-pressure single-crystal data. J Synchrotron Radiat 20:711–720. https://doi.org/10.1107/S0909049513018621
33. Shatskiy A, Sharygin IS, Litasov KD et al (2013) New experimental data on phase relations for the system Na2CO3-CaCO3 at 6 GPa and 900–1400 C. Am Mineral 98:2164–2171. https://doi.org/10.2138/am.2013.4436
34. Shen G, Wang Y, Dewaele A et al (2020) Toward an international practical pressure scale: A proposal for an IPPS ruby gauge (IPPS-Ruby2020). High Press Res 1–16. https://doi.org/10.1080/08957959.2020.1791107
35. Thomson AR, Walter MJ, Kohn SC, Brooker RA (2016) Slab melting as a barrier to deep carbon subduction. Nature 529:76–79. https://doi.org/10.1038/nature16174
36. Van Velthuizen J, Gault RA, Grice JD (1995) Calcioburbankite, Na 3 (Ca,REE,Sr) 3 (CO 3) 5, a new mineral species from Mont Saint-Hilaire, Quebec, and its relationship to the burbankite group of minerals. Can

Mineral 33:1231–1235

37. Zou G, Ye N, Huang L, Lin X (2011) Alkaline-Alkaline Earth Fluoride Carbonate Crystals ABCO3F (A = K, Rb, Cs; B = Ca, Sr, Ba) as Nonlinear Optical Materials. J Am Chem Soc 133:20001–20007. https://doi.org/10.1021/ja209276a
38. Zwolak JW, Boggs PT, Watson LT (2007) Algorithm 869: ODRPACK95: A weighted orthogonal distance regression code with bound constraints. ACM Trans Math Softw 33:27. https://doi.org/10.1145/1268776.1268782

Figures

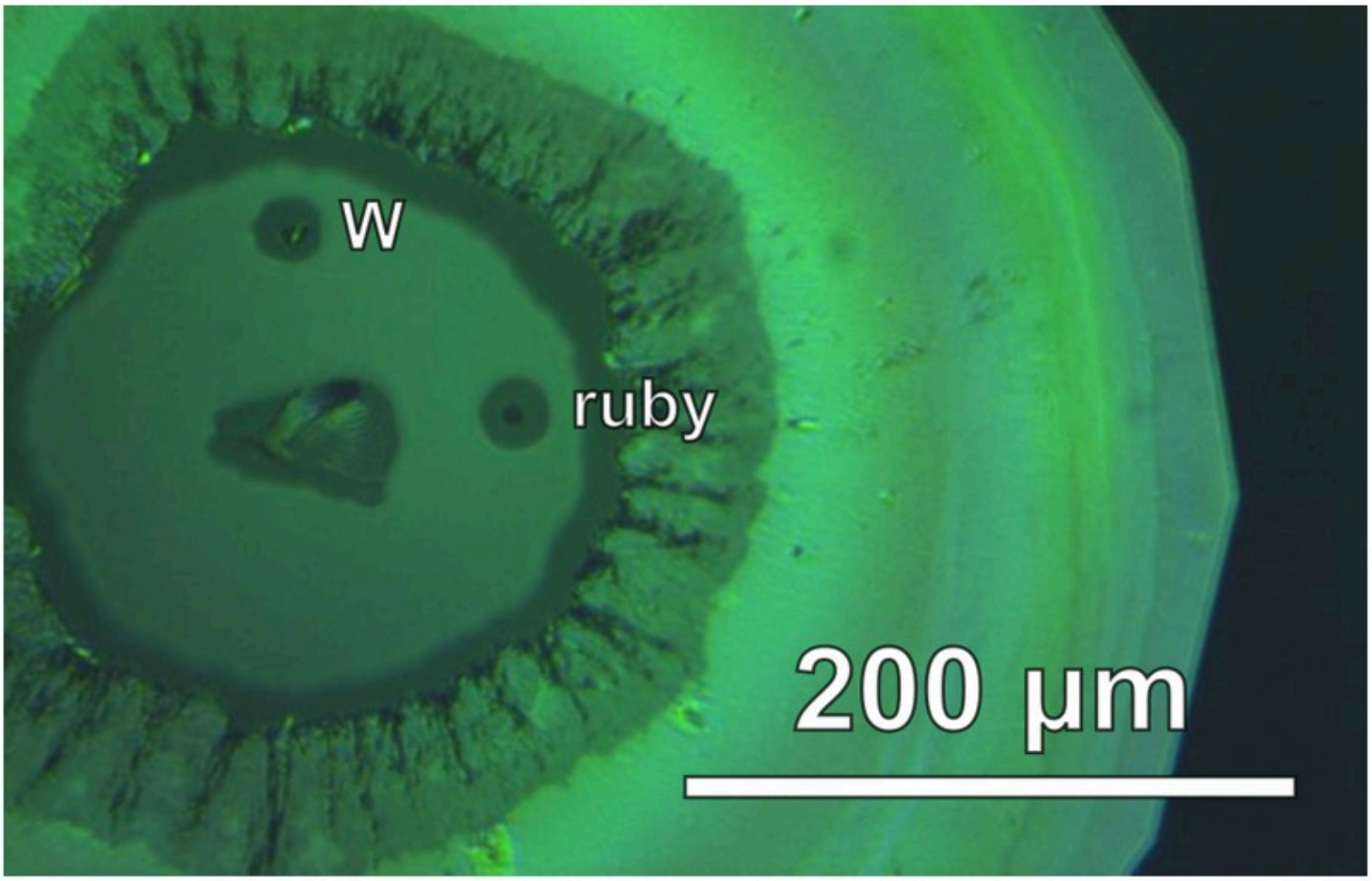


Figure 1

DAC sample chamber at ~10 GPa

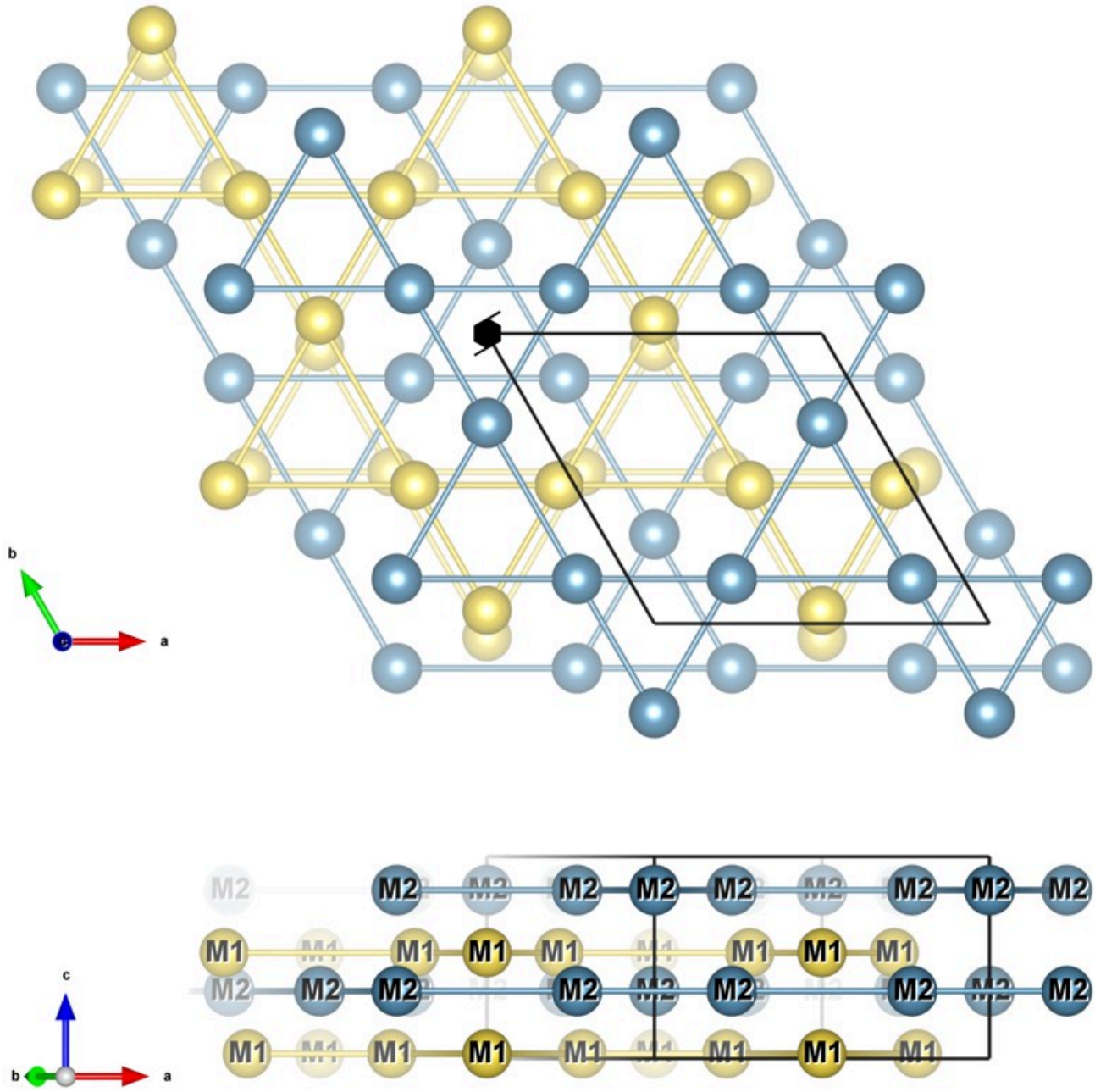


Figure 2

Kagome cation nets in calcioburbankite structure

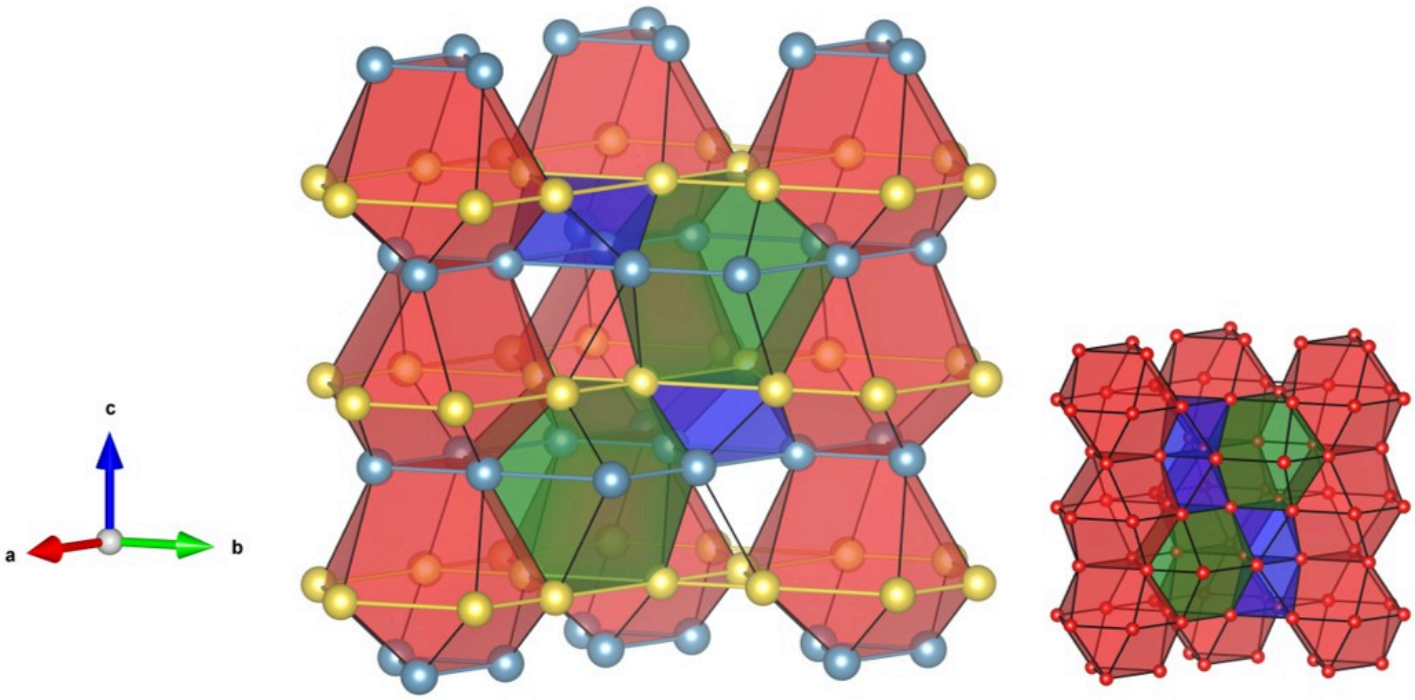


Figure 3

Left: $Na_2Ca_4(CO_3)_5$ structure ‘stretched’ along the *c* direction; right: α-$SrMnO_3$ 4H-perovskite

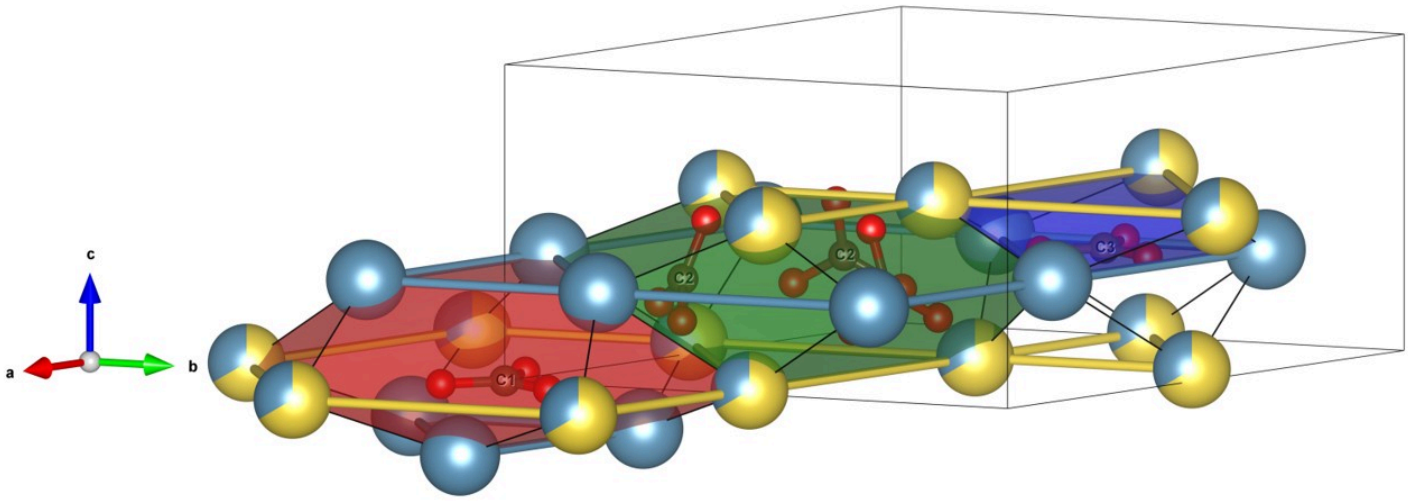


Figure 4

Occupation of tiles in $Na_2Ca_4(CO_3)$ structure by $(CO_3)^{2-}$ anions (population of M1 cation site by Na and Ca is shown by color)

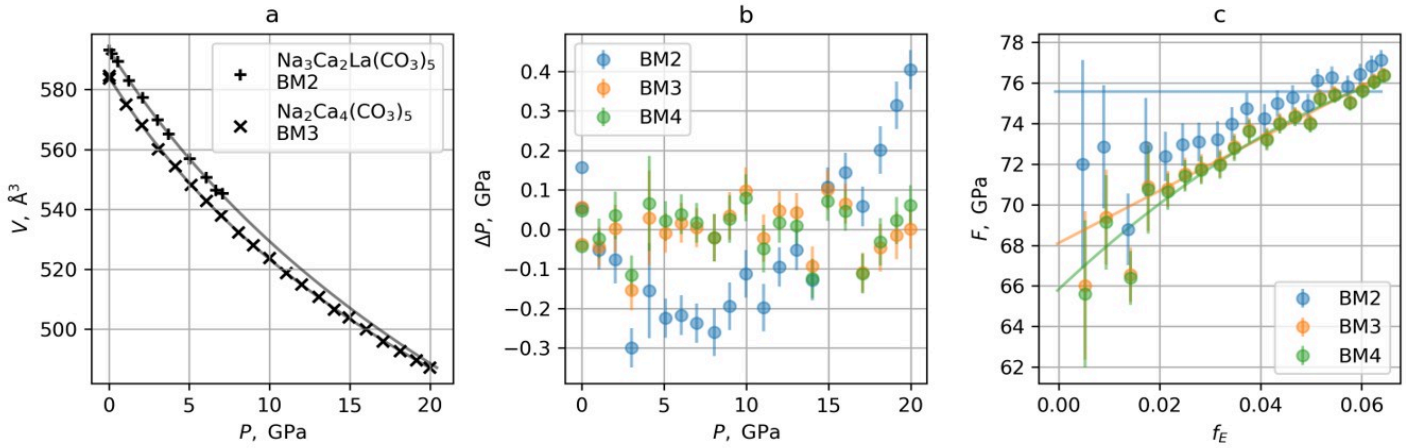


Figure 5

(a): *PV*-data for $Na_3Ca_2La(CO_3)_5$ and REE-free $Na_2Ca_4(CO_3)_5$ calcioburbankites; (b): deviation of observed pressures from EoS-predicted for $Na_2Ca_4(CO_3)$; (c): normalized pressure *vs.* finite Eulerian strain (‘*F-f*’) plots for $Na_2Ca_4(CO_3)$ equations of state. BM2-BM4 labels correspond to different orders of Birch-Murnaghan EoS.

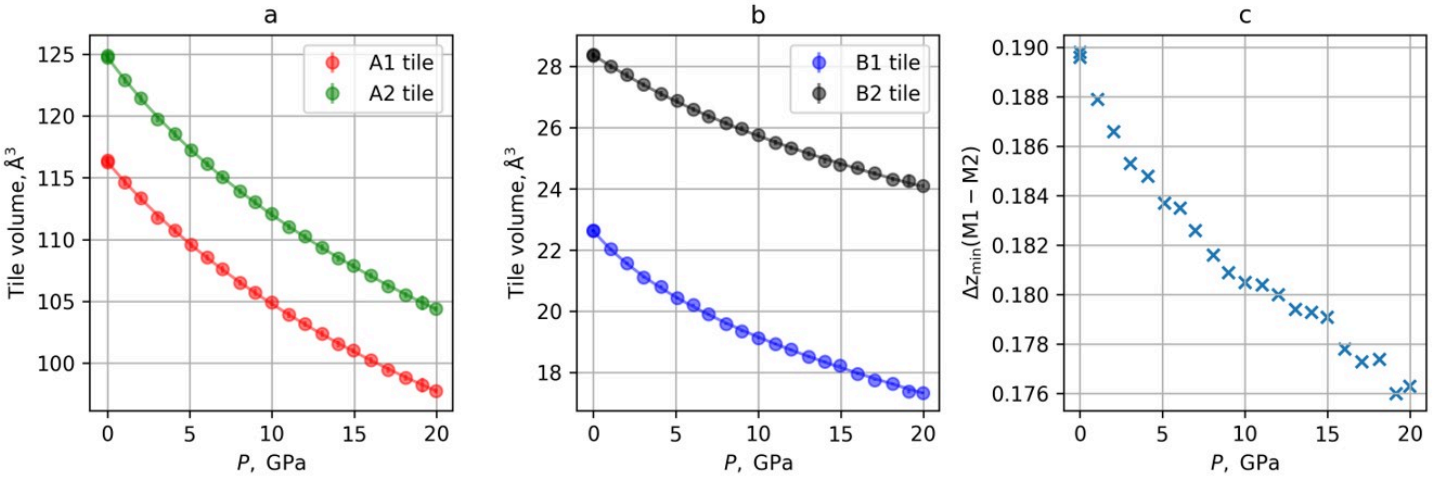


Figure 6

(a-b): compressibility of deformed cuboctahedral and octahedral tiles in $Na_2Ca_4(CO_3)_5$ structure;
(c): difference in *z* coordinate of the closest M1 and M2 kagome nets.

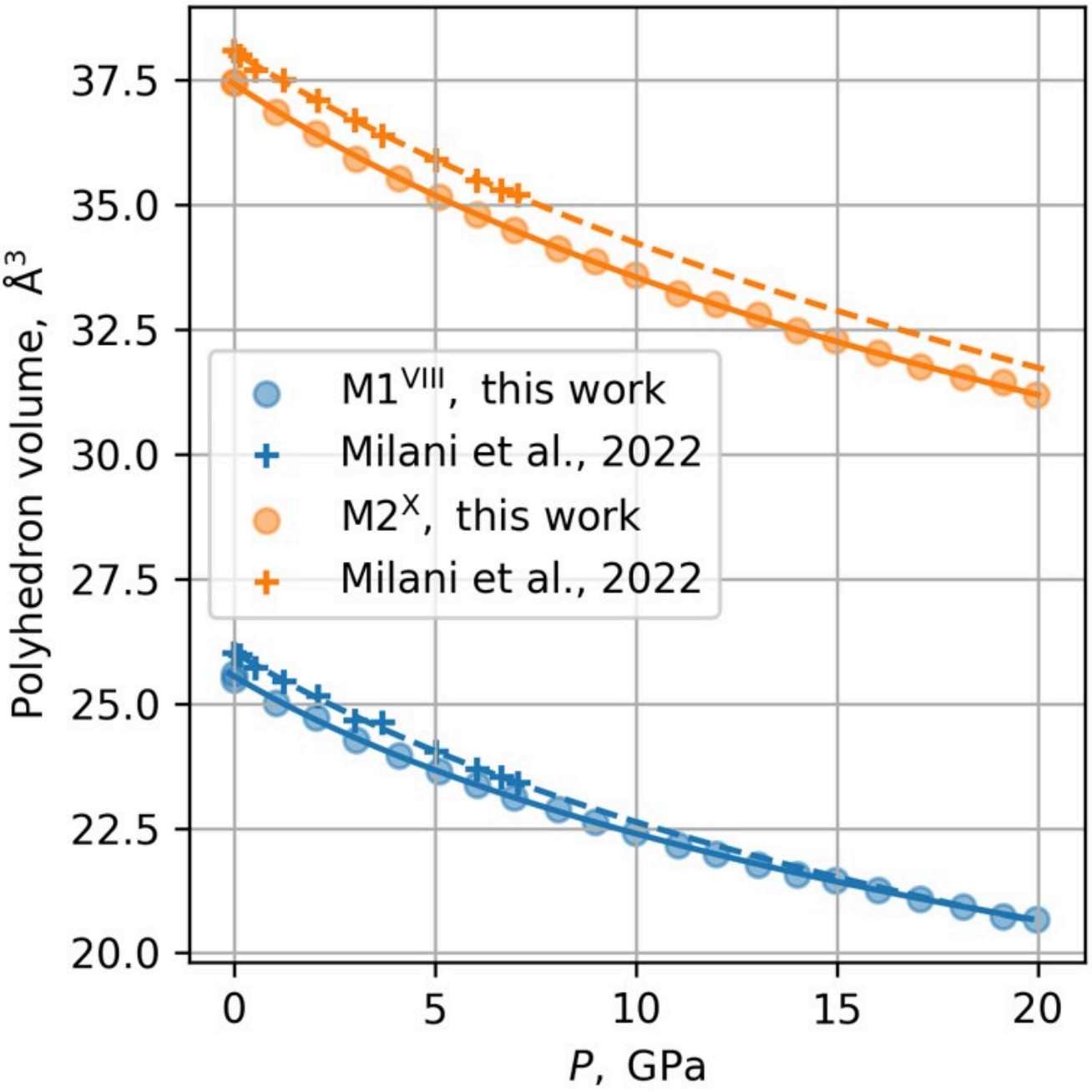


Figure 7

Compressibility of $M1O_8$ and $M2O_{10}$ coordination polyhedra in $Na_2Ca_4(CO_3)_5$ calcioburbankite

Supplementary Files

This is a list of supplementary files associated with this preprint. Click to download.

- Na2Ca4mergedNEW.cif
- checkcifNEW.pdf